

Simple realization of balanced motions under different speeds for a mechanical regulator-free bicycle robot

Yonghua Huang*, Qizheng Liao, Lei Guo and Shimin Wei

School of Automation, Beijing University of Posts and Telecommunications, Beijing 100876, China

(Accepted April 15, 2014. First published online: May 15, 2014)

SUMMARY

Mechanical regulator-free bicycle robots have lighter weight and fewer actuators than the traditional regulator-based bicycle robots. In order to deal with the difficulty of maintaining balance for this kind of bicycle robot, we consider a front-wheel drive and mechanical regulator-free bicycle robot. We present the methodologies for realizing the robot's ultra-low-speed track-stand motion, moderate-speed circular motion and high-speed rectilinear motion. A simplified dynamics of the robot is developed using three independent velocities. From the dynamics, we suggest there may be an underactuated rolling angle in the system. Our balancing strategies are inspired by human riders' experience, and our control rules are based on the bicycle system's underactuated dynamics. In the case of track-stand and circular motion, we linearize the frame's rolling angle and configure the robot to maintain balance by the front-wheel's motion with a fixed front-bar turning angle. In the case of the rectilinear motion, we linearize both front-bar steering angle and front-wheel rotating angle, and configure the system to maintain balance by the front-bar's turning with a constant front-wheel rotating rate. Numerical simulations and physical experiments are given together to validate the effectiveness of our control strategies in realizing the robot's proposed three motions.

KEYWORDS: Bicycle robot; Mechanical regulator-free; Track-stand motion; Circular motion; Rectilinear motion.

1. Introduction

The bicycle robot (unmanned bicycle) has the advantages of simple structure, energy savings and running capability in a narrow road, so it can potentially be used when performing field exploration, security patrol, entertainment exhibition etc.

Essentially, bicycle robots are statically unstable systems, so the primary obstacle to realize their developed function is dynamically falling over. In the past two decades, regulating the falling has been a challenging topic in the field of bicycle robot research, and there are, in summary, the following two types of regulators used in dealing with this issue:

- Type I: Regulator-based means.

Beznos *et al.*¹ proposed an autonomous bicycle with two gyros. They believed that when the two gyros span opposite directions, their gyroscopic torque due to the precession of gyros would counteract the destabilizing torque due to the gravity force. Lee and Ham² developed a movable load mass in their unmanned bicycle design. They suggested the following control strategy. If the bicycle falls left or right, by driving the center of the load mass right or left, the system would return back to the stable state because its center of gravity has been regulated by the load mass movement. As opposed to the mass balancer of Lee and Ham,² Yamakita *et al.*^{3,4} focused on a rotational balancer in their autonomous bicycle design. They stated that, due to momentum conservation, the rotation of their balancer in

* Corresponding author. E-mail: huangyonghuaxj@sina.com

direction opposite to the tilting angle could generate enough regulating torque to compensate for the tilting torque (induced by the gravity force). It is important to mention that Yamakita's group^{5,6} successfully developed a prototype for an ultra-low-speed standing. Yavin⁷ presented two kinds of innovative mechanical regulators, namely rotational bar and fly-wheel, to adjust his riderless bicycle's leaning angle. Yavin⁷ suggested that the symmetric bar or flywheel should not change the mass distribution of his bicycle when it is rotating, so it would be more convenient for maintaining bicycle's balance. Bui *et al.*⁸ were also concerned with the flywheel regulator in their design, and what is amazing is that their robot achieved a stable balance with zero moving velocity in a real experiment. Suebsomran⁹ proposed upper and lower flywheels in their bicycle robot design. In a simulation, they showed that the flywheels' rotation produced a suitable torque to stabilize the bicycle in a given roll angle. The most exciting achievement of the flywheel-based bicycle robot may be the Murata Boy robot.¹⁰ The naughty boy rode on a little bicycle, standing still, tracking a curve and even climbing a slope, as if by magic. As a compromise between the flywheels and mass balancers, Keo *et al.*¹¹ and Kawaguchi and Yamakita¹² presented a variable structure mechanical regulator in their riderless bicycle scheme. Their regulator is configured as a flywheel when the robot's leaning disturbances are large, and it will switch to a mass balancer when the position of the center of gravity is shifted. Keo *et al.*¹¹ claimed that the flywheel should perform better than the balancer in stabilizing his riderless bicycle. But he also recognized that the flywheel cannot cause his bicycle to track in the desired direction as the balancer can do. Both numerical simulations and physical experiments are shown to verify their ideas.

- Type II: Front-bar-based means.

Getz,^{13–15} Tanaka and Murakami¹⁶, Han *et al.*¹⁷ and Saguchi *et al.*^{18,19} insisted that a bicycle robot can be stabilized only by steering. Especially, using physical experiments, Saguchi *et al.*¹⁸ argued that the steering might be more efficient than the mechanical regulator in maintaining a bicycle robot's balance. Suryanarayanan *et al.*²⁰ concentrated on a riderless bicycle at high speed. They proposed that the front-bar's turning would exert dominant effects on bicycle's balance. Astrom *et al.*,²¹ Yi and Song²² and Zhang and Yi²³ believed that the front-fork's turning can regulate the bicycle robot's leaning angle by states feedback loops and the turning magnitude might depend on the robot's running velocity. Moreover, Astrom *et al.*²¹ suggested a lower bound for velocity, i.e., as long as the bicycle robot runs faster than this limit, it can easily be stabilized. Defoort and Murakami^{24,25} and Guo *et al.*²⁶ also balanced their own bicycle robot's motion in a short time just by the front-bar's turning. Yamaguchi²⁷ developed an intelligent system with a miniature humanoid robot riding a miniature bicycle. In his prototype experiments, the robot can perform stable balanced running with a turning handlebar and can stop bicycle by moving its feet from pedals to the ground. Yang *et al.*²⁸ concentrated their effort on the circular motion's simulation for an unmanned bicycle. In their idea, the bicycle can keep a stable balance by steering if an angular velocity of a rear-wheel is given. Yang *et al.*²⁸ pointed out that there is only one equilibrium point when the bicycle runs straight, whereas there may be many equilibrium points when the bicycle performs turning. Wang *et al.*²⁹ presented an evolutionary opinion that both balance and direction of an autonomous bicycle can be achieved only by the use of the handlebar steering. In order to testify their idea, scenario road tests for their bicycle were performed, and their results were convincing. Soudbakhsh *et al.*³⁰ focused on the human neuro-balance control of a stationary bicycle. With a lot of physical tests, they validated that it is impossible to stabilize stationary bicycle by only using rider's upper body movements. However, a rider can use steering as an additional actuation while incorporating his upper body movement to balance a stationary bicycle. Cerone *et al.*³¹ paid their attention to the balance abilities of a riderless bicycle against exogenous disturbances, such as a side wind gust and a slight slap on rear frame. Their physical prototype experiments validated the effectiveness of steering control to stabilize a running bicycle even when there are some external disturbances.

As mentioned above, the most distinctive properties of regulator-based bicycle robots may be whether they are configured with translational mass balancers or with rotational flywheels. More mechanisms and actuators are needed in this case. These changes lead to increase in systems' weight and energy consumption. Obviously, the situation does not agree with the original intention of lightweight and energy saving designs of bicycle robots. Another disadvantage for regulator-based bicycle robots may be the lack of fail-safe capability. If their mechanical regulators fail to work, this type of robot would be disabled from the normal work due to its over-dependence on the functional

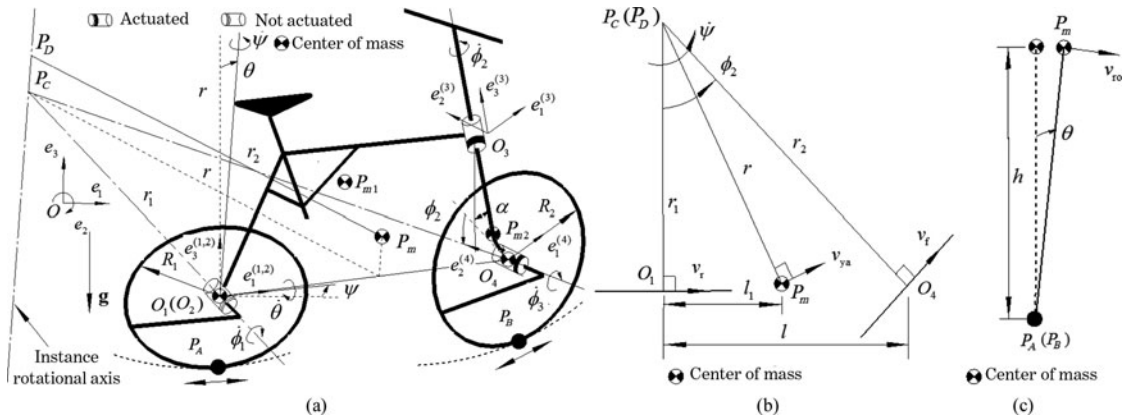


Fig. 1. Schematic diagram and kinematics analysis of a front-wheel drive bicycle robot which is free from mechanical regulators. (a) Front view of the robot showing the system’s coordinate frames settings and instantaneous rotational axis $P_C P_D$ etc. (b) Top view of the robot showing the horizontal velocities of the mass center, i.e., v_r , v_f and v_{ya} . (c) Side view of the robot showing the vertical velocities of the mass center, i.e., v_{to} .

action of regulators. As for the front-bar-based bicycle robots, the main problem by far is that there is no sufficient evidence; particularly, there are not enough convincing physical experiments to prove that this type of bicycle robot as well as regulator-based robot has the ability to perform the same balanced motions.

In this paper, we first aim to evaluate the self-balanced capability of a mechanical regulator-free bicycle robot when it runs at various speeds, and second we intend to improve the regulators fail-safe ability for regulator-based bicycle robots. In Section 2, a simplified dynamics is introduced by analyzing the instantaneous turning radius of a robot. In Section 3, we propose controllers for three balanced motions. In Sections 4 and 5, simulated and physical experiments are addressed to verify the feasibility of our control strategies. In the final section, we outline the conclusions for the whole paper and give the ideas about our future work.

2. Dynamic Model

Our work concentrates on a front-wheel drive robotic bicycle. The robot is not configured with any mechanical regulators. The schematic diagram of the robot is shown in Fig. 1.

In Fig. 1, $O_1(O_4)$ denotes the geometric center of the rear-wheel (front-wheel). P_m , P_{m1} and P_{m2} denote the mass center of the whole bicycle, the frame and the front-bar respectively. $P_A(P_B)$ denotes the ground contact point of the rear-wheel (front-wheel). P_C denotes the intersection point of rear- and front-wheels’ rotation axis. $P_C P_D$ is normal to $\Delta O_1 O_4 P_C$, so it can be treated as the frame’s instantaneous axis of rotation. Table I gives the physical meaning of the notations given in Fig. 1.

Figure 1 also shows the following coordinate systems of the robot:

- $O - e_1 e_2 e_3$ is the coordinate system fixed on the ground.
- $O_1 - e_1^{(1)} e_2^{(1)} e_3^{(1)}$ represents the coordinate system of the frame, and its origin is located at the geometric center of the rear-wheel.
- $O_2 - e_1^{(2)} e_2^{(2)} e_3^{(2)}$ represents the coordinate system fixed on the rear-wheel and its origin is also located at the geometric center of the rear-wheel.
- $O_3 - e_1^{(3)} e_2^{(3)} e_3^{(3)}$ is the coordinate system fixed on the front-bar, and its origin is located at the intersection point of the frame’s axis and the front-bar’s axis.
- $O_4 - e_1^{(4)} e_2^{(4)} e_3^{(4)}$ is the coordinate system fixed on the front-wheel and its origin is located at the geometric center of the front-wheel.

First, we consider the geometric relationship depicted in Fig. 1(b), and second, we formulate r_1 , r_2 and r as a function of l , l_1 and ϕ_2 : $r_1 = l \cot(\phi_2)$, $r_2 = l / \sin(\phi_2)$ and $r = \sqrt{l_1^2 + r_1^2} =$

Table I. Nomenclature.

| Parameter | Definition |
|------------------------|---|
| h | Height of P_m when the robot stands upright. |
| α | Offset angle between the vertical line and the front-bar axis when the robot stands upright. |
| R_1, R_2 | Rear-wheel's radius, front-wheel's radius. |
| r_1, r_2, r | Distance from O_1 to $P_C P_D$, distance from O_2 to $P_C P_D$, distance from P_{m1} to $P_C P_D$. |
| l, l_1 | Horizontal distance from O_1 to O_4 , horizontal distance from O_1 to the front-wheel's center P_m . |
| $\psi, \dot{\psi}$ | Yaw angle, yaw rate of the frame. |
| $\theta, \dot{\theta}$ | Roll angle, roll rate of the frame. |
| $\phi, \dot{\phi}$ | Pitch angle, pitch rate of the frame. |
| $\phi_1, \dot{\phi}_1$ | Rotational angle, rotational rate of the rear-wheel relative to the fame. |
| $\phi_2, \dot{\phi}_2$ | Rotational angle, rotational rate of the front-bar relative to the fame. |
| $\phi_3, \dot{\phi}_3$ | Rotational angle, rotational rate of the front-wheel relative to the front-bar. |
| v_f, v_r | Linear velocity of O_4 ; linear velocity of O_1 . |
| v_{ya}, v_{ro} | Part of linear velocity of P_m induced by the frame's turning; part of linear velocity of P_m induced by the frame's rolling. |

$\sqrt{l_1^2 + l^2 \cot^2(\phi_2)}$. Since we assume that the front-wheel runs on the ground without slipping, v_f can be represented as $R_2 \dot{\phi}_3$. On the other hand, we suppose that point O_4 rotates about line $P_C P_D$, so v_f can also be represented as $r_2 \dot{\psi}$. By combining these two analytical expressions of v_f , we can represent $\dot{\psi}$ as a function of $\dot{\phi}_3$: $\dot{\psi} = (R_2/l) \sin(\phi_2) \dot{\phi}_3$. Similarly, we consider the linear velocity of point O_1 , and then represent $\dot{\phi}_1$ as a function of $\dot{\phi}_3$: $\dot{\phi}_1 = (R_2/R_1) \cos(\phi_2) \dot{\phi}_3$.

As illustrated in Figs. 1(b) and (c), the linear velocity of P_m can be decomposed into two orthotropic parts, i.e.,

$$\begin{cases} v_{ro} = h\dot{\theta} \\ v_{ya} = r\dot{\psi} \end{cases} \tag{1}$$

We suppose the bicycle robot runs on a level ground with an invariable frame's pitch angle, so we can neglect its pitching rate and calculate frame's angular velocity vector as

$$\omega_{B_1} = \dot{\theta} e_1^{(1)} + \sin(\theta) \dot{\psi} e_2^{(1)} + \cos(\theta) \dot{\psi} e_3^{(1)}, \tag{2}$$

where $e_i^{(1)}$ ($i = 1, 2, 3$) is the i th axis basis vector in the frame coordinate system $O_1 - e_1^{(1)} e_2^{(1)} e_3^{(1)}$.

Moreover, we consider the relative motion between the frame and the front-bar, and then we calculate the front-bar's angular velocity,

$$\omega_{B_3} = {}^3_1 R \omega_{B_1} + \dot{\phi}_2 e_3^{(3)}, \tag{3}$$

where $e_3^{(3)}$ is the 3rd axis basis vector in the front-bar coordinate system $O_3 - e_1^{(3)} e_2^{(3)} e_3^{(3)}$; ${}^3_1 R$ represents the matrix of rotation transformation between coordinate frame $O_3 - e_1^{(3)} e_2^{(3)} e_3^{(3)}$ and $O_1 - e_1^{(1)} e_2^{(1)} e_3^{(1)}$.

For simplifying the analysis, the system's kinetic energy E_k is intentionally divided into two independent parts, i.e., rotation inducing energy and translation inducing energy. For the former, it is formulated as

$$\begin{cases} E_{k1} = (\omega_{B_1}^T \mathbf{J}_{B_1} \omega_{B_1} + J_{2yy} \dot{\phi}_1^2) / 2 \\ E_{k2} = (\omega_{B_3}^T \mathbf{J}_{B_3} \omega_{B_3} + J_{4yy} \dot{\phi}_3^2) / 2 \end{cases} \tag{4}$$

where \mathbf{J}_{B_1} denotes the inertial matrix of the assembly of the rear-wheel and the frame. \mathbf{J}_{B_3} denotes the inertial matrix of the assembly of the front-bar and the front-wheel. J_{2yy} and J_{4yy} denote rear-wheel's and front-wheel's moment of inertia around their own joint axis respectively. For the latter, we take

the whole system as an integral, yielding

$$E_{k3} = m(v_{ya}^2 + v_{ro}^2)/2, \quad (5)$$

where m represents the mass of the bicycle robot.

The total kinetic energy E_k of our system is defined as the algebraic sum of E_{ki} ($i = 1, 2, 3$). According to the previous analysis, $\dot{\psi}$ and $\dot{\phi}_1$ are the functions of $\dot{\phi}_3$, thus our system's total kinetic energy E_k can be explicitly calculated by the use of angular velocities $\dot{\theta}$, $\dot{\phi}_2$ and $\dot{\phi}_3$. The final expression of E_k shows that there are no explicit ψ , φ and ϕ_1 (ϕ_3) in the total kinetic energy.

In order to calculate our system's potential energy E_p , we assume that the turning of the front-bar cannot change the height of the mass center of the whole system, so we get

$$E_p = mgh \cos(\theta). \quad (6)$$

In our research, we only considered the track-stand motion, the circular motion and the rectilinear motion. For the former two motions, the front-bar is locked at a fixed angle, thus ϕ_2 , $\sin(\phi_2)$ and $\cos(\phi_2)$ become constant values. For the later motion, ϕ_2 is very small, then $\sin(\phi_2) \approx 0$ and $\cos(\phi_2) \approx 1$. No matter which case it will be, the two non-holonomic velocity constraints: $\dot{\psi} = (R_2/l) \sin(\phi_2) \dot{\phi}_3$, $\dot{\phi}_1 = (R_2/R_1) \cos(\phi_2) \dot{\phi}_3$ could be integrated to two holonomic geometric constrains:

$$\begin{cases} \phi_1 = (R_2/R_1) \cos(\phi_2) [\phi_3(t) - \phi_3(0)] \\ \psi = (R_2/l) \sin(\phi_2) [\phi_3(t) - \phi_3(0)] \end{cases},$$

where $\phi_3(0)$ is the initial angle of the front-wheel.

Besides, we suppose the bicycle robot runs with an invariable frame's pitch angle, so φ is also subjected to a holonomic geometric constrain. As a result, we can remove states variables, ψ , φ and ϕ_1 , from our system, and then choose the remaining variables θ , ϕ_2 and ϕ_3 as general coordinates for our system.

With E_k and E_p , we can calculate the Lagrange function: $L = E_k - E_p$. We substitute L into the Lagrange's equation,

$$\tau_i = \frac{d}{dt} \left(\frac{\partial L}{\partial \dot{q}_i} \right) - \frac{\partial L}{\partial q_i},$$

where q_i ($i = 1, \dots$) represents general coordinates.

Then our system's dynamic model can be

$$D(\theta) \ddot{\theta} + C(\theta, \dot{\theta}) \dot{\theta} + G(\theta) = \tau, \quad (7)$$

where $\theta = (\theta \ \phi_2 \ \phi_3)^T$ and $\tau = (0 \ \tau_1 \ \tau_2)^T$, which denote joint variables and joint driving torques respectively. $D_{3 \times 3}$ denotes the inertial matrix, and its elements are the functions of θ and ϕ_2 . $C_{3 \times 3}$ denotes the items relating to the Coriolis force etc., and its elements are the functions of θ , ϕ_2 , $\dot{\theta}$, $\dot{\phi}_2$ and $\dot{\phi}_3$. $G = (-mgh \sin(\theta) \ 0 \ 0)^T$, which denotes the item relating to the force of gravity.

Equation (7) reveals that our robot is an underactuated system with three independent velocities, and the frame's rolling angle is the underactuated degree of freedom.

3. Controller for Balanced Motions

As a consequence of Brockett's theorem,³² one cannot linearize all the state variables of a underactuated system by state feedback or nonlinear transformations, so we use the partial feedback linearization method to develop three balanced motion controllers for our bicycle robot.

3.1. Controller for track-stand motion

Track-stand motion is standing on the ground with zero running velocity. We get the inspiration from the human rider's balancing skills: holding the front-bar immobile and driving the wheels forward and backward to maintain balance. So we assume the front-bar of our bicycle to be locked at a fixed

angle position (here without loss of the generality, we use 45°. Other angles have similar results) and the system maintains balance by the front-wheel’s motion. In response to this case, the dynamics in Eq. (7) should be reduced, yielding

$$D_1(\theta_1)\ddot{\theta}_1 + C_1(\theta_1, \dot{\theta}_1)\dot{\theta}_1 + G_1(\theta_1) = \tau_1, \tag{8}$$

in which $\theta_1 = (\theta \ \phi_3)^T$, D_1 , C_1 , G_1 , θ_1 and τ_1 have the reduced forms of the corresponding items in Eq. (7).

First, we solve the first formula of Eq. (8) and get $\ddot{\phi}_3$. Second, we substitute the derived result of $\ddot{\phi}_3$ into the second formula of Eq. (8) and employ

$$\tau_2 = \left(d_{31} - \frac{d_{11}d_{33}}{d_{13}}\right)v + \left(c_{31} - \frac{c_{11}d_{33}}{d_{13}}\right)\dot{\theta} + \left(c_{33} - \frac{c_{13}d_{33}}{d_{13}}\right)\dot{\phi}_3 + \frac{d_{33}}{d_{13}}mgh \sin(\theta), \tag{9}$$

where v is a newly introduced virtual control variable; $c_{ij}(d_{ij})$ ($i, j = 1, \dots$) are the i th row and j th column element of the matrix $C_1(D_1)$. After the procedures, we can linearize the system’s underactuated roll angle θ . We set the system expectations θ^d and ϕ_3^d to zero and introduce symbols e_i ($i = 1, \dots, 4$) to denote the errors of $\theta, \dot{\theta}, \phi_3$ and $\dot{\phi}_3$. If we define the system’s output y to be the function of e_i ($i = 1, 3$) and employ the virtual control input

$$v = -k_p e_1 - k_d e_2 - k_1 e_4 - k_2 e_3, \tag{10}$$

where k_p, k_d, k_1 and k_2 represent the feedback coefficients of the state variables e_i ($i = 1, \dots, 4$) respectively, then we can formulate the system’s error affine equations as

$$\begin{cases} \dot{e} = f(e) + g(e)v \\ y = h(e) \end{cases}, \tag{11}$$

Where $e = (e_1 \ e_2 \ e_3 \ e_4)^T$, $y = (e_1 \ e_3)^T$, $f(e), h(e)$ and $g(e)$ are the vector functions of e , and

$$f(e) = \begin{pmatrix} e_2 \\ -k_d e_2 - k_p e_1 - k_1 e_4 - k_2 e_3 \\ e_4 \\ (ghm \sin e_1 - c_{11}e_2 - c_{13}e_4)/d_{13} \end{pmatrix},$$

$$g(e) = \begin{pmatrix} 0 \\ 0 \\ 0 \\ -d_{11}/d_{13} \end{pmatrix}, \quad h(e) = \begin{pmatrix} e_1 \\ e_3 \end{pmatrix}.$$

Next, we discuss the control system’s stability. From Eq. (11), we get the Jacobin matrix at equilibrium point ($e = 0$):

$$\frac{\partial \dot{e}}{\partial e} \Big|_{e=0} = \begin{pmatrix} 0 & 1 & 0 & 0 \\ -k_p & -k_d & -k_2 & -k_1 \\ 0 & 0 & 0 & 1 \\ w & 0 & 0 & 0 \end{pmatrix}, \tag{12}$$

where w is the quantity relative to mass, moment of inertia, structural parameters and the front-bar’s fixed turning angle. The secular equation of matrix (12) is described as

$$D(s) = s^4 + k_d s^3 + k_p s^2 + wk_1 s + wk_2 = 0. \tag{13}$$

According to the algebraic stability criterion, the necessary and sufficient condition of stability for the system of Eq. (11) can be described as that where all the coefficients in Eq. (13) are simultaneously

positive and satisfy the relationship:

$$k_d k_p - w k_1 > k_d^2 k_2 / k_1. \tag{14}$$

3.2. *Controller for circular motion*

Referring to the human rider’s experience in tracking a circle, we find that the human rider would not turn the handle-bar but control the driven wheel’s velocity to maintain balance. So we lock the front-bar at 45° and employ the driving torque as in Eq. (9). Besides, we only consider the uniform circular motion, so the resultant moment (about $P_A P_B$) due to the gravity and the centripetal force should be zero, which leads to

$$m a^{(n)} h \cos(\theta) - m g h \sin(\theta) = 0, \tag{15}$$

Where $a^{(n)}$ denotes the centripetal acceleration of P_m . Moreover, since $a^{(n)}$ is proportional to the square of $\dot{\psi}$, and $\dot{\psi}$ is the function of $\dot{\phi}_3$, Eq. (15) can also be expressed as

$$\dot{\phi}_3 = \sqrt{\lambda \tan(|\theta|)}, \tag{16}$$

where λ is a constant that relates the system’s geometric parameters, the acceleration of gravity and the front-bar’s turning angle etc.; $||$ is the absolute value operator.

We set the expectation $\theta^d = c$ and use $e_i (i = 1, 2, 3)$ to represent the errors of $\theta, \dot{\theta}$ and $\dot{\phi}_3$. If we define the output of our system to be $\mathbf{y} = (e_1 \ e_2 \ e_3)^T$ and employ

$$v = \ddot{\theta}^d - k_d e_2 - k_p e_1 - k_1 e_3, \tag{17}$$

where k_d, k_p and k_1 represent the feedback coefficients of the state variables $e_i (i = 1, 2, 3)$ respectively, we can get the system’s errors affine equation similar to Eq. (11), where $\mathbf{e} = (e_1 \ e_2 \ e_3)^T, \mathbf{y} = (e_1 \ e_2 \ e_3)^T, \mathbf{f}(\mathbf{e}), \mathbf{h}(\mathbf{e})$ and $\mathbf{g}(\mathbf{e})$ are the vector functions of \mathbf{e} , and

$$\mathbf{f}(\mathbf{e}) = \begin{pmatrix} e_2 \\ -k_d e_2 - k_p e_1 - k_1 e_3 \\ (ghm \sin(e_1 + c) - c_{11} e_2 - c_{13} e_3) / d_{13} \end{pmatrix},$$

$$\mathbf{g}(\mathbf{e}) = \begin{pmatrix} 0 \\ 0 \\ -d_{11} / d_{13} \end{pmatrix}, \quad \mathbf{h}(\mathbf{e}) = \begin{pmatrix} e_1 \\ e_2 \\ e_3 \end{pmatrix}.$$

Finally, with the same procedure performed in the track-stand motion, we can derive the necessary and sufficient condition of stability for circular motion, i.e.,

$$\begin{cases} k_d > w_2 \\ (k_d - w_2)(k_p - k_d w_2) > (k_1 w_1 - k_p w_2) > 0 \end{cases} \tag{18}$$

Where $w_i (i = 1, 2)$ is the quantity with respect to the inertial parameters, the geometrical parameters and the front-bar’s turning angle of the system.

3.3. *Controller for rectilinear motion*

We all know, the human rider can drive a bicycle to track a straight line approximately by turning the front-bar under various running velocities, and moreover, the faster the bicycle runs, the easier is the line-tracking action. Referring to this riding experience, we design a controller for rectilinear motion by turning the front-bar under a fixed front-wheel’s running velocity.

First, we rewrite Eq. (7) as

$$\begin{pmatrix} \mathbf{M}_{11} & \mathbf{M}_{12} \\ \mathbf{M}_{21} & \mathbf{M}_{22} \end{pmatrix} \begin{pmatrix} \ddot{\Theta}_1 \\ \ddot{\Theta}_2 \end{pmatrix} + \begin{pmatrix} \mathbf{F}_1 \\ \mathbf{F}_2 \end{pmatrix} = \begin{pmatrix} \tau_a \\ 0 \end{pmatrix}, \tag{19}$$

where $\Theta_1 = (\phi_2 \ \phi_3)^T$, $\Theta_2 = \theta$, $\tau_a = (\tau_1 \ \tau_2)^T$; M_{ij} ($i = 1, 2$) is the inertial matrix of appropriate dimension. F_i ($i = 1, 2$) is the quantity, including the Coriolis force and the gravity etc.

Then we linearize Θ_1 , and employ the driving torque

$$\tau_a = (M_{11} - M_{12}M_{22}^{-1}M_{21})v - M_{12}M_{22}^{-1}F_2 + F_1. \tag{20}$$

Next, we set expectations $\theta^d = 0$, $\phi_2^d = 0$ and $\phi_3^d = c$, and introduce e_i ($i = 1, \dots, 6$) to denote the errors of ϕ_2 , ϕ_2 , ϕ_3 , ϕ_3 , θ and $\dot{\theta}$. If we define the output y of our system as a function of errors e_1 , e_3 and e_5 , and employ

$$v = -k_1e_1 - k_2e_2, \tag{21}$$

where k_1 and k_2 are the feedback coefficient matrices defined as $k_1 = \begin{pmatrix} k_{p1} & k_{d1} & 0 & 0 \\ 0 & 0 & k_{p2} & k_{d2} \end{pmatrix}$, $k_2 = \begin{pmatrix} k_1 & k_2 \\ 0 & 0 \end{pmatrix}$, and $k_1, k_2, k_{p1}, k_{p2}, k_{d1}$ and k_{d2} denote the feedback coefficients of the state variables e_i , vectors $e_1 = (e_1 \ e_2 \ e_3 \ e_4)^T$, $e_2 = (e_5 \ e_6)^T$, we can also derive the system's error affine equations similar to the form shown in Eq. (11):

$$\begin{cases} \dot{e}_1 = Ae_1 + p(e_1, e_2) \\ \dot{e}_2 = f(e_1, e_2) \\ y = h(e_1, e_2) \end{cases},$$

where

$$A = \begin{pmatrix} 0 & 1 & 0 & 0 \\ -k_{p1} & -k_{d1} & 0 & 0 \\ 0 & 0 & 0 & 1 \\ 0 & 0 & -k_{p2} & -k_{d2} \end{pmatrix}, \quad p(e_1, e_2) = \begin{pmatrix} 0 \\ ke_6 \\ 0 \\ 0 \end{pmatrix},$$

$$f(e_1, e_2) = \begin{pmatrix} e_6 \\ f \end{pmatrix}, \quad h(e_1, e_2) = \begin{pmatrix} e_1 \\ e_3 \\ e_5 \end{pmatrix},$$

$$f = -d_{11}^{-1}[d_{12}(-k_{d1}e_2 - k_{p1}e_1 + k_2e_6) + d_{13}(-k_{d2}e_4 - k_{p2}e_3) \dots + c_{11}e_6 + c_{12}e_2 + c_{13}(e_4 + c) - ghm \sin(e_5)].$$

Similarly, based on the eigenvalue analysis of the corresponding Jacobin matrix, we also obtain the necessary and sufficient condition of stability of this kind of balance motion as:

$$\begin{cases} k_1, k_2 < 0 \\ ((k_{p1} - k_{p2})^2 + k_{p2}k_{d1}^2 + k_{p1}k_{d2}^2) + k_{d1}k_{d2}(k_{p2} + k_{p1}) > 0 \\ k_{d2} + k_{d1}, k_{p1}k_{p2} > 0, k_{d2}k_{p2} + k_{d2}^2k_{d1} + k_{d1}^2k_{d2} + k_{d1}k_{p1} > 0 \end{cases}. \tag{22}$$

4. Control Simulations

In this section, we will conduct numerical simulations of three kinds of balanced motions by the use of the controllers proposed in last section.

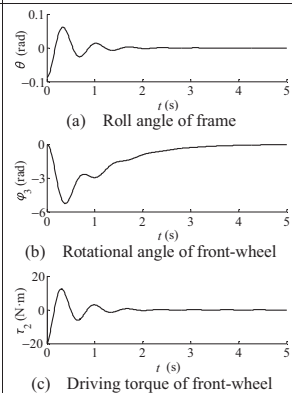
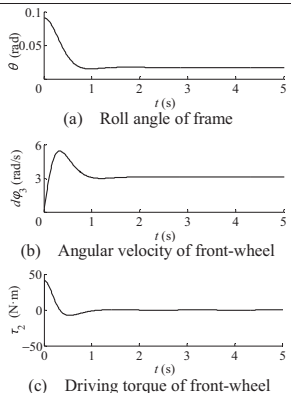
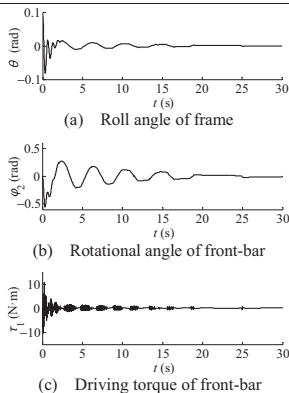
Table II illustrates the structural parameters that are needed in our simulations. These parameters are obtained from the estimation of a virtual prototype rather than the identification of our physical prototype, but these are still used in our following prototype experiments.

We consider the controllers' necessary and sufficient condition of stability in Eqs. (14), (18) and (22), and then set the states feedback coefficients as shown in line 2 of Table III. In the rectilinear motion, we only consider that the robot runs with a constant front-wheel velocity, rather than a time-variant one. We do this here for the sake of simplicity. As a consequence, the front-wheel's kinetic parameters would not provide feedback to our controller.

Table II. Parameters of the simulation.

| Sym | Physical meanings | Value |
|-----------|--|---|
| h | Height of mass center (m) | 0.41 |
| α | Front-bar's offset angle | 20° |
| R_1 | Rear-wheel's radius (m) | 0.19 |
| R_2 | Front-wheel's radius (m) | 0.17 |
| l | Distance between the rear- and front-wheel's center (m) | 0.89 |
| l_1 | Distance between the mass center and the rear-wheel's center (m) | 0.51 |
| m | Mass of the robot (kg) | 21.34 |
| g | Acceleration of gravity (m/s ²) | 9.8 |
| J_{B1} | Inertia matrix of the assembly of rear-wheel and frame (kg·m ²) | $\begin{pmatrix} 0.236 & 0 & 0 \\ 0 & 2.143 & 0 \\ 0 & 0 & 1.384 \end{pmatrix}$ |
| J_{B2} | Inertia matrix of the assembly of front-bar and front-wheel (kg·m ²) | $\begin{pmatrix} 0.682 & 0 & 0 \\ 0 & 0.785 & 0 \\ 0 & 0 & 0.021 \end{pmatrix}$ |
| J_{2yy} | Inertia moment of rear-wheel around its rotational axis (kg·m ²) | 0.036 |
| J_{4yy} | Inertia moment of front-wheel around its rotational axis (kg·m ²) | 0.028 |

Table III. Simulated configurations and results.

| Motion type | Track-stand motion | Circular motion | Rectilinear motion |
|------------------------------------|---|--|---|
| Feedback coefficients | $k_p = 107, k_d = 8$ $k_1 = 0.155, k_2 = 0.126$ | $k_p = 30, k_d = 15$ $k_1 = 0.055$ | $k_{p1} = 120, k_{d1} = 5$ $k_1 = -0.03, k_2 = -0.0032$ |
| Result of the simulated experiment |  <p>(a) Roll angle of frame</p> <p>(b) Rotational angle of front-wheel</p> <p>(c) Driving torque of front-wheel</p> |  <p>(a) Roll angle of frame</p> <p>(b) Angular velocity of front-wheel</p> <p>(c) Driving torque of front-wheel</p> |  <p>(a) Roll angle of frame</p> <p>(b) Rotational angle of front-bar</p> <p>(c) Driving torque of front-bar</p> |

Line 3 in Table III shows three simulated experiment results. From these results we have:

- In track-stand motion (column 2 of line 3)

In column 2 of line 3 of Table III, Figure (a) shows the robot is initially set to tilt with -0.087 rad. Under the regulating actions of a balanced controller, the tilting angle gradually decreases, and after 4 s, the angle is limited to a narrow range of 0 rad. This phenomenon implies that the bicycle robot swings in the vicinity of its equilibrium position. In column 2 of line 3 of Table III, Figure (b) shows the front-wheel runs quickly to -5.24 rad in 0.4 s at the beginning, and then smoothly turns back to 0 rad. This phenomenon indicates that the robot eventually returns to its initial location. In column 2 of line 3 of Table III, Figure (c) shows the maximum front-wheel's driving torque is about -20 N·m, which would not be inaccessible for a normal DC motor.

- In circular motion (column 3 of line 3)

In column 3 of line 3 of Table III, Figure (a) shows the robot's initial tilting angle of 0.087 rad. When the controller operates, the tilting angle starts reducing, and about 2 s later, it converges to the anticipated 0.017 rad. In column 3 of line 3 of Table III, Figure (b) shows that the front-wheel turns the angular velocity to the prescribed 3.14 rad/s in 2 s. According to the moment equilibrium

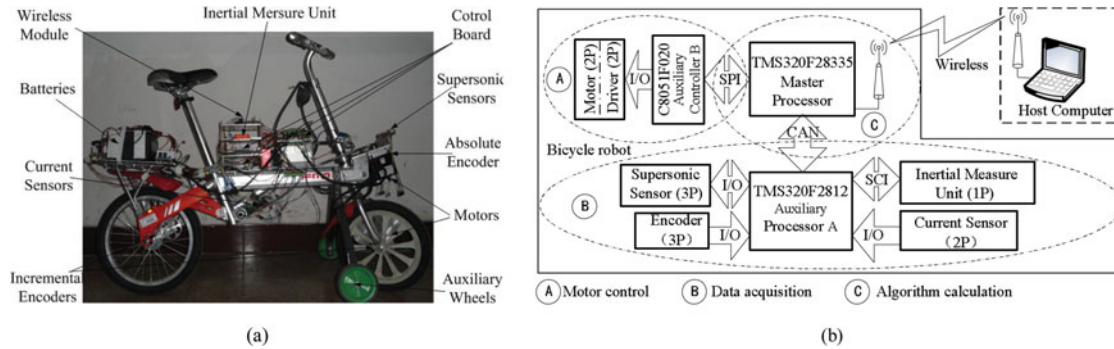


Fig. 2. Experimental prototype. (a) Overall layout of the robot. The robot is developed with four basic bones, i.e., the front-wheel, the rear-wheel, the frame and the front-bar. (b) Configuration of the autonomous driving system, including three key function modules, marked A, B and C, which serve as the motor control, the data acquisition and the algorithm calculation correspondingly.

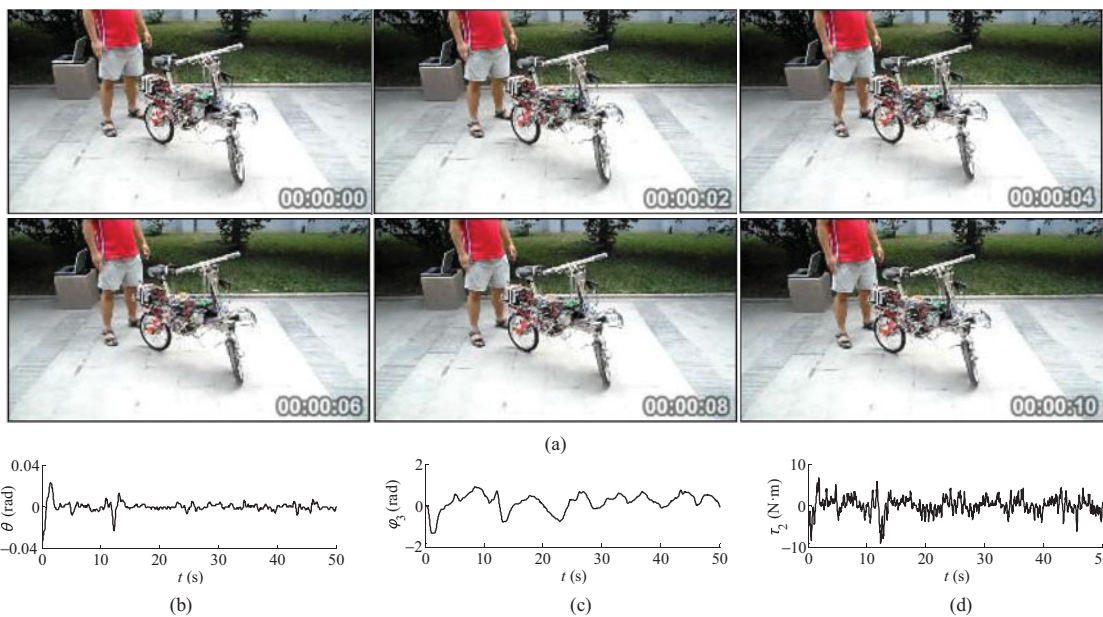


Fig. 3. Results of the track-stand motion experiment. (a) Snapshots of the experiment, which shows the bicycle robot stands stably for more than 10 s on a level ground. (b) Rolling angle of the frame, which shows that the robot is limited to a small range near the zero position. (c) Rotational angle of the front-wheel, which shows that the wheel runs with trivial displacement in its initial location. Figures (b) and (c) together verify that the robot performs the track-stand motion. (d) Driving torque of the front-wheel, which is limited to 10 N·m, is far lower than the actuated motor’s critical torque.

condition given in Eq. (16), we know that the system stays at the state of dynamic equilibrium. In column 3 of line 3 of Table III, Figure (c) shows that the maximum front-wheel’s driving torque is about 37.5 N·m, which can be achieved by a normal DC motor.

- In rectilinear motion (column 4 of line 3)

In column 4 of line 3 of Table III, Figure (a) shows that the robot’s initially tilting with -0.087 rad. The front-wheel’s angular velocity is set to 3π rad/s. Under the regulation of our controller, the tilting angle gradually falls, and after 20 s, it permanently stays at 0 rad. This situation shows that the robot runs stably on the ground. In column 4 of line 3 of Table III, Figure (b) shows the front-bar turns left and right frequently at the beginning, but it eventually decreases to 0 rad. This situation indicates that the robot system roughly runs in a straight line. In column 4 of line 3 of Table III, Figure (c) shows that the maximum driving torque of the front-bar is less than 10 N·m.

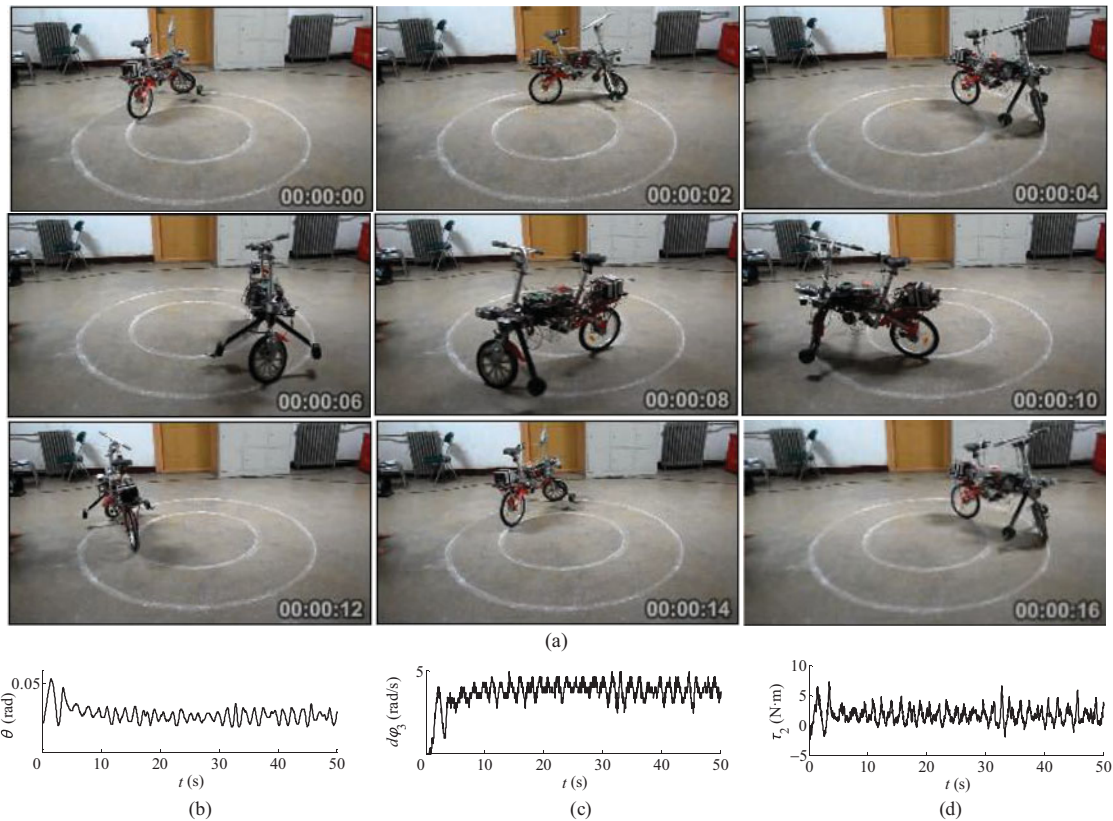


Fig. 4. Results of the circular motion experiment. (a) Snapshot of the experiment, which shows the robot running in a circle stably for less 16 s. (b) Rolling angle of the frame, which converges nearly to a constant eventually. (c) Angular velocity of the front-wheel, which converges nearly to a constant. Obviously, Figures (b) and (c) are consistent with the moment equilibrium condition in Eq. (16), which further shows that the robot runs in a circle. (d) Driving torque of the front-wheel, which is limited to ± 8 N·m and far lower than the actuated motor's critical torque.

As a consequence of the above discussion, we believe the bicycle robot achieves three kinds of balanced motions by respective controllers with reasonable torques.

5. Prototype Experiments

To testify the real effectiveness of our control strategies, a physical prototype, say BYBR-I, is developed. The prototype is actually 1.2 m in length, 0.7 m in height and 23 kg in weight.

5.1. Prototype hardware configuration

Figure 2(a) illustrates the overall framework of the prototype. Figure 2(b) shows the hardware configurations of the robot's control system.

As shown in Fig. 2, the developed prototype primarily consists of five parts, which are as follows:

- Control unit (Digital Signal Processor (DSP) + sensors)
- Communication unit (wireless modules)
- Support (aluminum alloy + steel)
- Actuation unit (DC servomotors)
- Accessories (batteries, auxiliary wheels)

The prototype should be developed to be as compact as possible, thus the DSP-based control board, the wireless module, most of the sensors and the batteries are attached to the prototype frame. Two DC servomotors are mounted on the front-wheel and front-bar's joints. The motors can easily drive the front-wheel and the front-bar thru gear reducers. In order to prevent the robot from falling over and damaging costly devices, a couple of auxiliary wheels are installed on the two sides of the robot, which are 15 cm from the floor when the robot stands erectly.

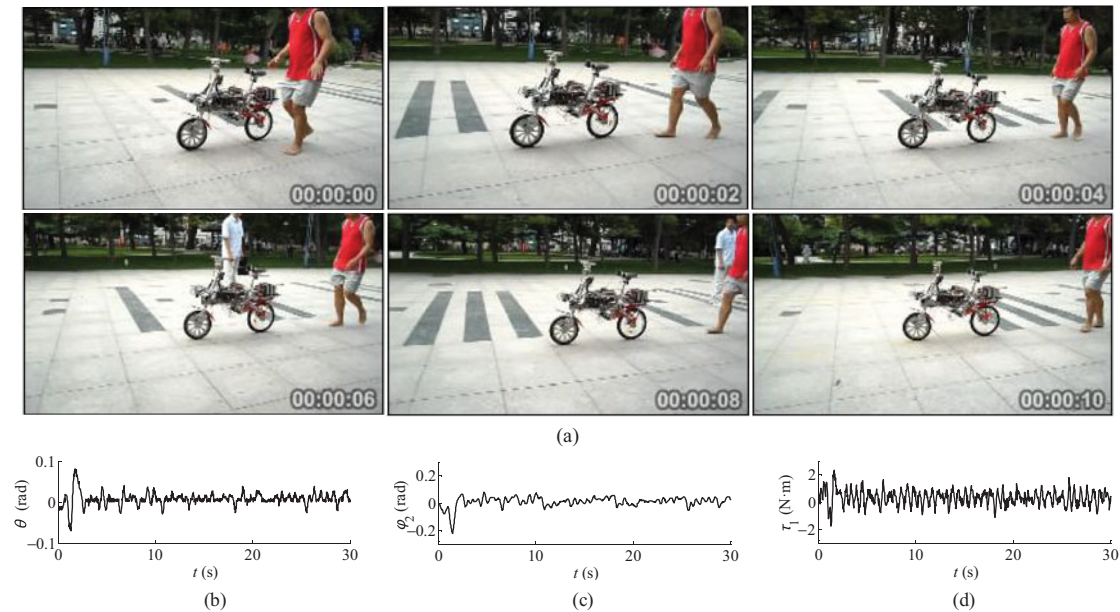


Fig. 5. Results of the rectilinear motion experiment. (a) Snapshot of the experiment, which shows the robot running a straight line stably for less 10 s. (b) Roll angle of the frame, which stays around zero. (c) Rotational angle of the front-bar, which stays around zero. Figures (b) and (c) together indicate that the robot runs stably in a straight line. (d) Driving torque of the front-bar, which is strictly limited to 3 N·m and far lower than the actuated motor's critical torque.

As shown in Fig. 2, we use two chips of DSPs (TMS320 F28335 and TMS320F2812) and a microcontroller (MCU) (C8051F020) in our system. For the sensors group, an Inertial Measure Unit (IMU) and three encoders are employed to get the posture information of the bicycle robot. In addition, three supersonic sensors and two current sensors are introduced for the detection of obstacles and the current measurements of motors respectively. Since the bicycle may run fast over long distance on the ground, we use a couple of wireless modules to transfer data between the host computer and the bicycle robot. But for short distances onboard microprocessors, we use CAN bus, SPI bus and SCI bus to exchange data.

From Fig. 2, we also see that there are four CPUs in the robot's control system. We divided this system into three hierarchies. The first one is the host computer, which is in charge of making the strategic decision and monitoring the whole system's state. The second one comprises two DSPs, which are responsible for the sensors' data acquisition and control algorithm calculation. The last one is MCU, which deals with the control of two motors. The working procedure of the control system can be summarized as follows:

- Step 1: The TMS320F28335 (DSP) sends a requirement message of data transferring to TMS320F2812 (DSP) for asking for sensors data.
- Step 2: The TMS320F2812 responds to the requirement message and returns the latest sensors data to F28335.
- Step 3: The TMS320F28335 calculates the needed control quantities according to the received sensors data, and sends them to the C8051F020 (MCU). After that, these control quantities together with the sensors data are transferred to the host computer.
- Step 4: The C8051F020 generates the corresponding driving signals according to the control quantities to drive the two motors.

5.2. Balanced motion experiments

The parameters used in our controllers are shown in Table II. Since there may be deviations between the real parameters and the estimated ones, we need to retune the states feedback coefficients. Next, we provide the three trials in detail.

- Motion A: Track-stand motion

Prior to the trial, we lock the front-bar at $\pi/4$ rad and reset the states feedback coefficients as: $k_d = 140$, $k_p = 187$, $k_1 = 5.3389$, $k_2 = 1.0268$.

Figure 3 shows the results of our track-stand experiment. Figure 3(a) gives the snapshots of the experiment, which shows that the bicycle robot operates stably for longer than 10 s. Figure 3(b) shows that the robot's rolling angle is strictly limited to a small range near to the equilibrium point, and a slight disturbance, which happens at 12 s, does not disrupt the system's balance at all. This case shows the abilities of our controller to compensate for the noise and disturbances. Figure 3(c) shows the front-wheel runs with a trivial displacement in its initial location. As a whole, Figs. 3(b) and (c) verify that the robot is operating in the track-stand motion. Figure 3(d) shows that the front-wheel's maximum driving torque is 9.6 N·m, which is about 39% of the driving motor's critical torque.

In conclusion, the robot prototype achieves well its track-stand motion.

- Motion B: Circular motion

We again lock the front-bar at $\pi/4$ rad and reset the state feedback coefficients as: $k_p = 160$, $k_d = 80$, $k_1 = 2.36$.

Figure 4 shows the results of this experiment. Figure 4(a) shows that the robot runs in a circular trajectory at about 14 s per round. Figure 4(b) shows, the robot's rolling angle converges to the prescribed value. Figure 4(c) shows that the front-wheel's velocity quickly rises to the preset value. These phenomena verify the moment equilibrium condition in Eq. (16). Figure 4(d) shows that the maximum of the front-wheel's driving torque is less than 10 N·m (10 N·m is about 40% of the driving motor's critical torque).

- Motion C: Rectilinear motion

We set free the previously locked front-bar and configure the controller's feedback coefficients as: $k_p = 100$, $k_d = 30$, $k_1 = -5.62$, $k_2 = -0.55$. Similar to the setup of velocity in rectilinear motion simulation, the driving angular velocity of the front-wheel is maintained at 3π rad/s.

Figure 5 shows the experimental results of the rectilinear motion. It is seen from Fig. 5(b) that the frame's rolling angle is strictly limited in the vicinity of 0 rad. This situation indicates that the robot is performing a balanced motion. Figure 5(c) shows that the front-bar's rotational angle is basically constrained at 0 rad and its biggest deviation is about 0.20 rad. This phenomenon implies that our robot runs in a trajectory close to a straight line. Figure 5(d) shows that the maximum value of the front-bar's driving torque is less than 3 N·m. This value is about 11.6% of the driving motor's critical torque.

Summarily, we can conclude from the analyses that our bicycle robot perfectly achieves its rectilinear motion.

As a whole, with the proposed controllers, we accomplish the three kinds of balanced motions' physical experiments. On the other hand, the three experimental results validated the practical effectiveness of our strategies.

6. Conclusions and Future Work

Maintaining balance is the most fundamental requirement for a bicycle robot. In the traditional views, most researchers believe that mechanical regulators are the best means to achieve a bicycle robot's balance. While for the bicycle robots which are free of mechanical regulators, they argue that it is difficult to maintain balance, especially in the case of low speed.

This paper is concerned with three kinds of balanced motions of a front-wheel drive and mechanical regulator-free bicycle robot when it runs in different speeds. For making a rule, we first present a simplified model for the proposed system. Our model can well symbolize the robot's coupling dynamics with three independent angular velocities and an underactuated rolling angle. Second, accounting for the underactuated characteristics of the dynamics, we develop model-based balanced controllers for the system's ultra-low-speed track-stand motion, moderate-speed circular motion and high-speed rectilinear motion. The main advantages of our controllers are that they are simple and compactly closed structures, which can be easily used in our microprocessor-based controlling system. Finally, with the proposed controllers, both simulations and physical experiments are performed to demonstrate that our bicycle robot can realize three motions with reasonable driving torques.

Our work indicates that mechanical regulator-free bicycle robots can also perform the same balanced motions in various speeds as the regulator-based ones do. Moreover, when the regulator-based bicycle robots are subjective to the mechanical regulator malfunction, by turning to the steering-balanced mode, our control strategies can be used to the fault-tolerance control for this kind of bicycle robots.

One limitation in our work is that our bicycle robot cannot automatically turn from one balanced motion state to another. For this reason, the extensions of our research should involve developing an autonomous switching strategy to perform smooth turning among the three motions. In addition, since the structural parameters, e.g., moment of inertia and mass, used in experimental controllers mainly stem from individual estimations, it is difficult to choose appropriate controller parameters just by the proposed theoretic stability conditions (Because the theoretic stability conditions completely depend on the accuracy of the structural parameters). So developing a strategy for controller parameters' self-tuning is also a significant work that should be done next. Finally, we should generalize our strategies to the regulator-based bicycle robots as a spare control method in future.

Acknowledgements

This work is funded by National Natural Science Foundation of China (grant No. 61105103) and Beijing Natural Science Foundation (grant No. 4132032). In addition, we would like to express our appreciations to Dr. Yuan Song from Robot Laboratory of Beijing University of Posts and Telecommunications for his unselfish help with physical experiments.

References

1. A. V. Beznos, A. M. Formalsky, E. V. Gurfinkel, D. N. Jicharev, A. V. Lensky, K. V. Savitsky and L. S. Tchesalin, "Control of Autonomous Motion of Two-Wheeled Bicycle with Gyroscopic Stabilization," *Proceedings of the IEEE International Conference on Robotics and Automation (ICRA)*, Leuven, Belgium, vol. 3 (May 16–20, 1998) pp. 2670–2675.
2. S. Lee and W. Ham, "Self Stabilizing Strategy in Tracking Control of Unmanned Electric Bicycle with Mass Balance," *Proceedings of the IEEE/RSJ International Conference on Intelligent Robots and Systems (IROS)*, Lausanne, Switzerland, vol. 3 (Oct. 2002) pp. 2200–2205.
3. M. Yamakita and A. Utano, "Automatic Control of Bicycles with a Balancer," *Proceedings of the IEEE International Conference on Advanced Intelligent Mechatronics (AIM)*, Monterey, California, USA (Jul. 24–28, 2005) pp. 1245–1250.
4. M. Yamakita, A. Utano and K. Sekiguchi, "Experimental Study of Automatic Control of Bicycle with Balancer," *Proceedings of the IEEE/RSJ International Conference on Intelligent Robots and Systems (IROS)*, Beijing, China (Oct. 9–15, 2006) pp. 5606–5611.
5. L. Keo and M. Yamakita, "Controlling Balancer and Steering for Bicycle Stabilization," *Proceedings of the IEEE/RSJ International Conference on Intelligent Robots and Systems (IROS)*, St. Louis, USA (Oct. 11–15, 2009) pp. 4541–4546.
6. L. Keo and M. Yamakita, "Control of an autonomous electric bicycle with both steering and balancer controls," *Adv. Robot.* **25**(1–2), 1–22 (2011).
7. Y. Yavin, "The derivation of a kinematic model from the dynamic model of the motion of a riderless bicycle," *Comput. Math. Appl.* **51**(6–7), 865–878 (2006).
8. T. T. Bui, M. Parnichkun and C. H. Le, "Structure-Specified H_∞ Loop Shaping Control for Balancing of Bicycle Robots: A Particle Swarm Optimization Approach," *Proc. Inst. Mech. Eng. J. Syst. Control Eng.* **224**(7), 857–867 (Nov. 2010).
9. A. Suebsomran, "Balancing Control of Bicycle Robot," *Proceedings of the IEEE International Conference on Cyber Technology in Automation, Control and Intelligent Systems (CYBER)*, Bangkok, Thailand (May 27–31, 2012) pp. 69–73.
10. Murata Manufacturing Co., Ltd, Bicycling robot "Murata boy." (Sep. 29, 2005) Available at: <http://www.murata.com.cn>, Accessed 15 December 2011.
11. L. Keo, K. Yoshino, M. Kawaguchi and M. Yamakita, "Experimental Results for Stabilizing of a Bicycle with a Flywheel Balancer," *Proceedings of the IEEE International Conference on Robotics and Automation*, Shanghai International Conference Center, Shanghai, China (May 9–13, 2011) pp. 6150–6155.
12. M. Kawaguchi and M. Yamakita, "Stabilizing of Bike Robot with Variable Configured Balancer," *Proceedings of the SICE Annual Conference*, Waseda University, Tokyo, Japan (Sep. 13–18, 2011) pp. 1057–1062.
13. N. H. Getz, "Control of Balance for a Nonlinear Nonholonomic Non-Minimum Phase Model of a Bicycle," *Proceedings of the American Control Conference (ACC)*, Baltimore, Maryland, vol. 1 (Jun. 29–Jul. 1, 1994) pp. 148–151.

14. N. H. Getz, "Internal Equilibrium Control of a Bicycle," *Proceedings of the 34th IEEE Conference on Decision and Control (CDC)*, New Orleans, LA, vol. 4 (Dec. 13–15, 1995) pp. 4285–4287.
15. N. H. Getz and J. E. Marsden, "Control for an Autonomous Bicycle," *Proceedings of the IEEE International Conference on Robotics and Automation (ICRA)*, Nagoya, Aichi, Japan, vol. 2 (May 21–27, 1995) pp. 1397–1402.
16. Y. Tanaka and T. Murakami, "Self Sustaining Bicycle Robot with Steering Controller," *Proceedings of the 8th IEEE International Workshop on Advanced Motion Control (AMC)*, Kawasaki, Japan (Mar. 25–28, 2004) pp. 193–197.
17. S. Han, J. Han and W. Ham, "Control algorithm for stabilization of tilt angle of unmanned electric bicycle," *Trans. Control Autom. Syst. Eng.* **3**(3), 176–180 (Sep. 2001).
18. T. Saguchi, K. Yoshida and M. Takahashi, "Stable running control of autonomous bicycle robot," *Trans. Japan Soc. Mech. Eng.* **73**(7), 2036–2041 (Jul. 2007).
19. T. Saguchi, M. Takahashi and K. Yoshida, "Stable running control of autonomous bicycle robot for trajectory tracking considering the running velocity," *Trans. Japan Soc. Mech. Eng.* **75**(750), 397–403 (Feb. 2009).
20. S. Suryanarayanan, M. Tomizuka and M. Weaver, "System Dynamics and Control of Bicycles at High Speeds," *Proceedings of the American Control Conference (ACC)*, Anchorage, AK, vol. 2 (May 8–10, 2002) pp. 845–850.
21. K. J. Astrom, R. E. Klein and A. Lennartsson, "Bicycle dynamics and control: Adapted bicycles for education and research," *IEEE Control Syst. Mag.* **25**(4), 26–47 (2005).
22. J. G. Yi, D. Z. Song, A. Levandowski and S. Jayasuriya, "Trajectory Tracking and Balance Stabilization Control of Autonomous Motorcycles," *Proceedings of the IEEE International Conference on Robotics and Automation (ICRA)*, Orlando, Florida (May 15–19, 2006) pp. 2583–2589.
23. Y. Z. Zhang and J. G. Yi, "Dynamic Modeling and Balance Control of Human/Bicycle Systems," *Proceedings of the IEEE/ASME International Conference on Advanced Intelligent Mechatronics (AIM)*, Montréal, Canada (Jul. 6–9, 2010) pp. 1385–1390.
24. M. Defoort and T. Murakami, "Second Order Sliding Mode Control with Disturbance Observer for Bicycle Stabilization," *Proceedings of the IEEE/RSJ International Conference on Intelligent Robots and Systems (IROS)*, Nice, France (Sep. 22–26, 2008) pp. 2822–2827.
25. M. Defoort and T. Murakami, "Sliding-mode control scheme for an intelligent bicycle," *IEEE Trans. Ind. Electron.* **56**(9), 3357–3368 (Sep. 2009).
26. L. Guo, Q. Z. Liao and S. M. Wei, "Dynamic modeling of bicycle robot and nonlinear control based on feedback linearization of MIMO systems," *J. Beijing Univ. Posts Telecommun.* **30**(1), 80–84 (2007).
27. M. Yamaguchi, "Miniature robot rides bicycle like a pro." (Nov. 13, 2011) Available at: <http://www.gizmag.com/yamaguchi-bicycle-riding/20478/>, Accessed 15 December 2011.
28. J. H. Yang, S. Y. Lee, S. Y. Kim, Y. S. Lee and O. K. Kwon, "Linear Controller Design for Circular Motion of Unmanned Bicycle," *Proceedings of the 11th International Conference on Control, Automation and Systems, KINTEX*, Gyeonggi-do, Korea (Oct. 16–29, 2011) pp. 893–897.
29. L. X. Wang, J. M. Eklund and V. Bhalla, "Simulation & Road Test Results on Balance and Directional Control of an Autonomous Bicycle," *Proceedings of the 25th IEEE Canadian Conference on Electrical and Computer Engineering (CCECE)*, Montreal, Canada (Apr. 29–May 2, 2012) pp. 1–5.
30. D. Soudbakhsh, Y. Zhang and J. Yi, "Stability Analysis of Human Rider's Balance Control of Stationary Bicycles," *Proceedings of the American Control Conference*, Fairmont Queen Elizabeth, Montréal, Canada (Jun. 27–29, 2012) pp. 2755–2760.
31. V. Cerone, D. Andreo, M. Larsson and D. Regruto, "Stabilization of a riderless bicycle," *IEEE Control Syst. Mag.* **30**(5), 23–32 (2010).
32. R. W. Brockett, "Asymptotic stability and feedback stabilization," *In: Differential Geometric Control Theory* (R. W. Brockett, R. S. Millman and H. J. Sussmann, eds.) (Birkhauser, Boston, MA, 1983) pp. 181–191.